ACS APPLIED ENERGY MATERIALS

www.acsaem.org Article

A High-Voltage Hybrid Solid Electrolyte Based on Polycaprolactone for High-Performance all-Solid-State Flexible Lithium Batteries

Yuhang Li, Min Liu, Shanshan Duan, Zixian Liu, Shuen Hou, Xiaocong Tian,* Guozhong Cao,* and Hongyun Jin*

Cite This: *ACS Appl. Energy Mater.* 2021, 4, 2318−2326 Read Online

ACCESS | Metrics & More | Article Recommendations | Supporting Information

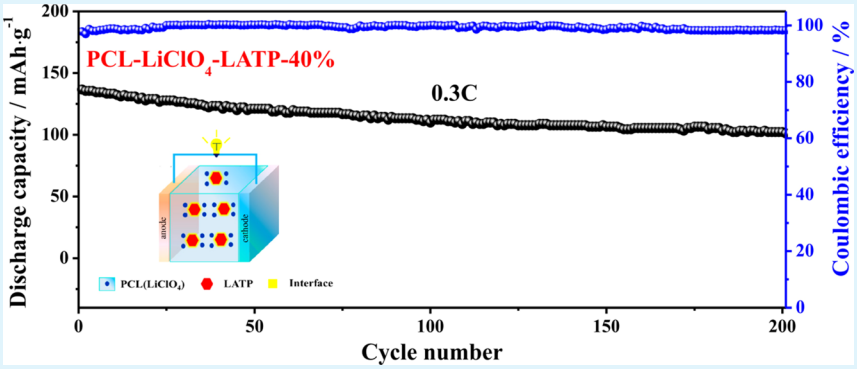

ABSTRACT: All-solid-state lithium batteries are promising to overcome the safety issues and limited energy density concern of commercial Li-ion batteries (LIBs). In this study, cubic-phase $Li_{1.4}Al_{0.4}Ti_{1.6}(PO_4)_3$ (LATP) powders are prepared and filled into biodegradable polycaprolactone (PCL) matrixes to form a flexible PCL−$LiClO_4$−LATP hybrid solid electrolytes (HSEs). Owing to the excellent electrochemical stability of the PCL matrix, the HSEs offer a wide electrochemical potential window of 5 V (vs Li/Li^+), an ionic conductivity of 3.64×10^{-5} S cm^{-1} at 55 °C, and a high Li-ion transference number of 0.58. In addition, the fabricated all-solid-state lithium batteries exhibit an outstanding electrochemical performance with a high initial discharge specific capacity of 136.6 mAh g^{-1} and a good capacity retention of 75% after 200 cycles at 0.3 C. The superior performance indicates that the HSEs with the PCL as the polymer matrix provide an inspiring approach to develop high-performance flexible and safe all-solid-state lithium batteries.

KEYWORDS: *all-solid-state lithium battery, hybrid solid electrolyte, polycaprolactone, high Li-ion transference number, high voltage*

1. INTRODUCTION

Massive efforts have been dedicated toward enhancing the energy density of Li-ion batteries (LIBs) because of the growing demand for electric vehicles and hybrid electric vehicles. Metallic lithium is one of the most promising anode candidates for LIBs, which has a high theoretical capacity (3860 mAh g^{-1}), a low density (0.535 g cm^{-3}), and the lowest negative potential (−3.04 V vs standard hydrogen electrode).[1−4] However, metallic lithium-based batteries using liquid organic electrolytes cannot form a stable and homogeneous solid electrolyte interphase (SEI).[5,6] Consequently, the SEI within these batteries is easily damaged irreversibly, and Li dendrites are formed rapidly, leading to a limited life span. More importantly, the liquid organic electrolyte is unfriendly to the environment and brings nonnegligible safety issues such as uncontrolled chemical reactions, flaming, leakage, internal short circuits, and even explosion. In comparison, solid-state electrolyte-based lithium batteries have attracted extensive research interest, thanks to the high energy density, high safety, and stable SEI layers with the lithium metal anode.[7−9] Solid-state electrolytes are thus highly desirable for next-generation battery electrolytes.[10,11] Among various solid-state electrolytes, hybrid solid electrolytes (HSEs), where the polymer matrix, lithium salt, and passive ceramic filler or active ceramic filler are basically contained, have showed high ionic conductivity and excellent electrochemical performance.[12−15] In a previous work, the liquid electrolyte was introduced into the all-solid-state lithium batteries for the improved interface infiltration between HSEs and electrodes.[16,17] The volume of the liquid electrolyte is typically overcommitted to promote the battery perform-

Received: November 13, 2020
Accepted: January 22, 2021
Published: March 4, 2021

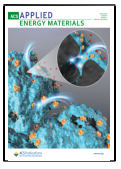

https://dx.doi.org/10.1021/acsaem.0c02846
ACS Appl. Energy Mater. 2021, 4, 2318−2326

ance, which are not believed as real all-solid-state lithium batteries.[18]

Poly(ethylene oxide) (PEO)-based HESs have been mostly investigated with varied kinds of lithium salt and additive particles in recent years, as it possesses a strong Li-ion solvating ability and a high chain flexibility for ion transport.[19,20] However, the narrow electrochemical stability window (<4 V vs Li/Li^+), low Li-ion transference number, and poisonous preparation processes of PEO-based electrolytes limit the development of all-solid-state lithium batteries.[21] As an alternative to PEO, polycaprolactone (PCL) is biodegradable, inexpensive, environment friendly, and involves low cost production, which can act as the ideal polymer matrix for HSEs. As a flexible chain, the structure of PCL is similar to that of PEO, and it has nonbonding electrons that can dissociate lithium salt easily, a low glass transition temperature (T_g) at −60 °C, and a wide electrochemical stability window (>5 V vs Li/Li^+).[22] Moreover, PCL exhibits brilliant thermal stability and mechanical properties that are critical parameters of a separator in LIBs. Fonseca et al. used PCL/$LiClO_4$ as the solid-state electrolyte to develop a biodegradable polymer electrolyte in an all-solid-state lithium battery for the first time in 2006.[23] Eriksson et al. fabricated HSEs based on PCL/TFSI/Al_2O_3, which exhibited good compatibility with electrodes in all-solid-state lithium batteries in 2019.[24] Additionally, some investigations paid attention to the copolymer of PCL and obtained favorable-performance solid-state electrolytes.[25−30] However, the solid-state electrolytes based on PCL also exhibit some drawbacks, such as a high degree of crystallinity and rate performance in all-solid-state lithium batteries.[31] Thus, it is a huge challenge for promoting the PCL-based solid-state electrolyte performance of batteries and making it possess the value of practical applications.

In this study, we report HSEs where $Li_{1.4}Al_{0.4}Ti_{1.6}(PO_4)_3$ (LATP) and $LiClO_4$ are both filled in the PCL matrix to improve the electrochemical performance. It is demonstrated that the preparation process of HSEs is uncomplicated, inexpensive, nonpoisonous, and accessible to large-scale production.[32,33] The optimized PCL−$LiClO_4$−LATP HSEs have a high Li-ion transference number (t_{Li+} = 0.58) which ensures the superior cycling performance and a stable interface between electrolytes and electrodes and offers a wide electrochemical potential window of 5 V vs Li/Li^+. Additionally, the percentage of the crystallinity of optimized PCL−$LiClO_4$−LATP HSEs is 26.48% that is lower than that of pure PCL (41.43%). Without using any liquid electrolyte, all-solid-state lithium batteries based on $LiFePO_4$ (LFP) presents a high discharge specific capacity of 149.0 mAh g^{-1} at 0.2 C at 55 °C and shows a prominent cycling performance of 75% capacity retention without distinct Li dendrite growth after 200 cycles at 0.3 C. The result also shows a significant cycling achievement, superior electrochemical stability, and interfacial wettability under high temperature conditions, which paves a new avenue for future inexpensive, environmentally friendly, high-performance solid-state electrolytes.

2. EXPERIMENTAL SECTION

2.1. Materials Preparation. Dimethyl carbonate (DMC), lithium perchlorate ($LiClO_4$), powders of TiO_2, Al_2O_3, Li_2CO_3, and $(NH_4)_2HPO_4$ were purchased from Aladdin, Shanghai (China). PCL was dried in a vacuum oven for 12 h at room temperature. The cathode material LFP and lithium metal were obtained from Tianjin STL Energy Technology Co.

Stoichiometric amounts of TiO_2, Al_2O_3, Li_2CO_3, and $(NH_4)_2HPO_4$ were used as the starting materials to prepare LATP using a conventional solid solution method.[34] The mixture was heated to 700 °C for 1 h to ensure the complete decomposition of $(NH_4)_2HPO_4$ and Li_2CO_3 and then continued to be heated to 900 °C for 2 h in order to accomplish the melting and homogenization processes. Subsequently, the ceramic powders were prepared by ball milling for 6 h, and the obtained sample was LATP particles that were stored in an Ar-filled glovebox for further electrochemical tests. The phases of the LATP particles are shown in Figure S1.

PCL and $LiClO_4$ were dissolved in anhydrous DMC by magnetic stirring at O/Li = 20 (the molar ratio). The mixed solution was stirred for 6 h at 60 °C. Then, different LATP particle contents of 20 and 40 wt % were added as fillers into the solution, and it was further stirred continuously for 6 h at 55 °C to disperse homogeneously. Afterward, the solution was casted onto the glass plate using a coater, and the resultant HSEs membrane was dried for 12 h at room temperature in order to evaporate the solvent. The membrane of HSEs was cut into circular pieces with a diameter of 19 mm and placed in an Ar-filled glovebox for electrochemical measurements and assembly of all-solid-state lithium batteries. Additionally, PCL−$LiClO_4$−LATP-20% and PCL−$LiClO_4$−LATP−40% were denoted as HSEs-20% and HSEs-40%, respectively.

2.2. Characterization and Electrochemical Measurements of HSEs. The morphology and the element distribution of HSEs were characterized by scanning electron microscopy (SEM, HITACHI SU8010) and energy-dispersive spectrometry (EDS). The phases of samples were examined using $CuK_{\alpha 1}$ radiation (λ = 0.15405 nm) with a D8-ADVANCE X-ray diffractometer. Thermogravimetric analysis (TGA) was performed on a STA 449 F3 thermal analyzer with a heating rate of 10 °C min^{-1} from room temperature to 900 °C in a N_2 atmosphere. Differential scanning calorimetry (DSC) characterizations were performed to investigate the melting temperature (T_m) and the percentage of crystallinity (χ_c) for different electrolyte membranes. The crystallinities (χ_c) of the HSEs could be calculated according to the following formula:

$$\chi_c = \Delta H_m / \Delta H_{PCL} * (1 - \varphi_{add}) * 100\% \quad (1)$$

where ΔH_m and ΔH_{PCL} (139.3 J g^{-1})[35] are the melting enthalpies for the samples and pure PCL matrix with 100% crystallinity, and φ_{add} is the total weight percentage of additives (lithium salt and nanoparticles).[24,36,37]

The ionic conductivities of HSEs were determined via electrochemical impedance spectroscopy (EIS). An alternating current (AC) amplitude of 5 mV was imposed, and the measurements were achieved with a frequency from 10 M Hz to 0.1 Hz at various temperatures using a Zahner electrochemical workstation. The HSE membrane was sandwiched between two stainless-steel (*SS*) blocking electrodes to construct SS| PCL−$LiClO_4$−LATP |SS batteries.[38] The resistance value associated with the membrane conductivity was determined according to the following formula:

$$\sigma = L / RS \quad (2)$$

where *L*, *R*, and *S* stand for the film thickness, the total resistance, and the area of the HSE membrane, respectively.[6,39] The thickness of the HSE membrane is ∼120 μm. The battery was determined by the Zahner electrochemical workstation from 30 to 75 °C.

To investigate the electrochemical stability window of HSEs, the measurement was assessed using the linear sweep voltammetry (LSV) technique from 1.0 to 5.0 V at a scan rate of 1 mV s^{-1}. Then, an SS electrode played a part of a working electrode, and Li metal was utilized as a reference and counter electrode (Li| PCL−$LiClO_4$−LATP |SS). The Li-ion transference number measurement of HSEs-20% and HSEs-40% was conducted in a Li| PCL−$LiClO_4$−LATP |Li battery system that was polarized with a direct current(DC) voltage of 5 mV. The Li-ion transference number was tested using the following Bruce−Vincent formula:

https://dx.doi.org/10.1021/acsaem.0c02846
ACS Appl. Energy Mater. 2021, 4, 2318−2326

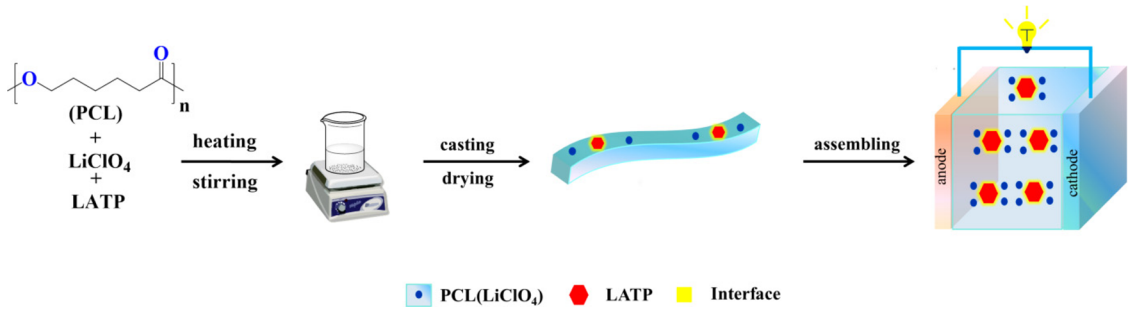

Figure 1. Schematic illustration of HSE fabrication.

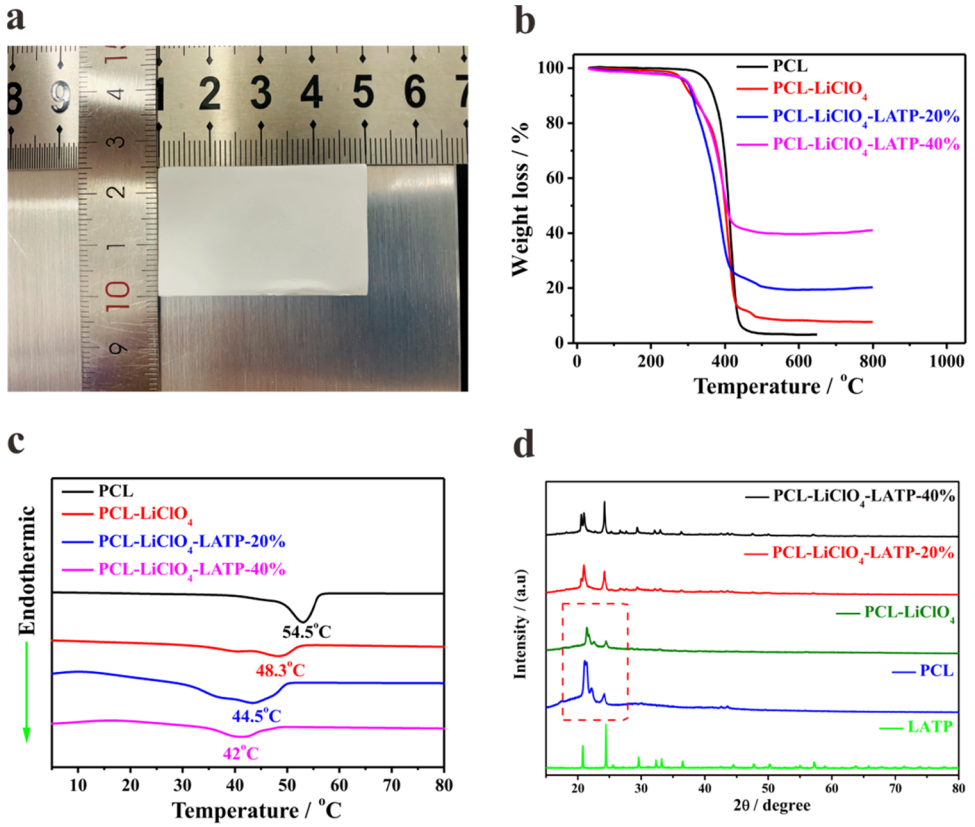

Figure 2. (a) Photograph of the membrane of HSEs-40%. (b) TG curves of the PCL, PCL−$LiClO_4$, HSEs-20%, and HSEs-40%. (c) DSC curves of the PCL, PCL−$LiClO_4$, HSEs-20%, and HSEs-40%. (d) XRD patterns of LATP, PCL, PCL−$LiClO_4$, HSEs-20%, and HSEs-40%.

$$t_{Li^+} = \frac{I_{SS}(\Delta V - I_0 R_0)}{I_0(\Delta V - I_{SS} R_{SS})} \quad (3)$$

where ΔV is the potential applied across the battery (5 mV in this case), I_0 and I_{SS} are the initial and steady-state currents, respectively, and R_0 and R_{SS} represent the initial interfacial resistance and the steady-state interfacial resistance of the passivating layers on the lithium metal electrodes, respectively.[40,41] The interface compatibility and stability between the HSEs and lithium metal electrodes were examined by Li| PCL−$LiClO_4$−LATP |Li symmetric batteries, and the symmetric batteries were tested at 55 °C. A galvanostatic cycling of the Li| PCL−$LiClO_4$−LATP |Li battery was charged and discharged for 1 h alternately to further investigate the interface stability and suppression of Li dendrite formation by introducing a current density of 0.12 mA cm^{-2}.[42−46]

2.3. Electrochemical Measurement of all-Solid-State Lithium Batteries. The cathode in the all-solid-state lithium battery was composed of 60 wt % LFP, 20 wt % super-P and 20 wt % polyvinylidene fluoride, whose slurry was dispersed homogenously and coated on an aluminum foil. Then, the coated cathode was dried in vacuum at 60 °C for 24 h in order to remove traces of the remaining solvent. The lithium metal with a diameter of 16 mm served as the anode. The loading of the LFP active material on the cathode was controlled at 0.90−1.20 mg cm^{-2}, and the cathode film was cut into circular pieces with a diameter of 15 mm. The CR 2032-type LFP| PCL-$LiClO_4$-LATP |Li battery was assembled in an Ar-filled glovebox. The batteries were subjected to a temperature of 55 °C for 1.5 h to improve the interface compatibility and were activated by a low rate in the initial few cycles. The cycling performance and rate capability (0.2~2C) of the all-solid-state lithium batteries was investigated using a Neware CT-4008 battery testing system at 55 °C with the voltage range of 2.5~4.2 V (vs Li/Li^+). The EIS of all-solid-state lithium batteries was explored with a frequency from 10 M Hz to 0.1 Hz using a Zahner electrochemical workstation by applying 5 mV AC amplitude at 55 °C.

3. RESULTS AND DISCUSSION

The HSEs were prepared via solution casting, as shown in Figure 1. The preparation process is simple and highly

https://dx.doi.org/10.1021/acsaem.0c02846
ACS Appl. Energy Mater. 2021, 4, 2318−2326

repeatable, indicating the ease of large-scale fabrication. The excellent mechanical property and thermal stability of HSEs are facilitative to the industrial production and reducing the risk of short circuiting when operating at high temperatures. The photographic images of the obtained HSE film after solution casting and the corresponding thermal stability are displayed in Figure 2a,b, respectively. The initial weight loss of 3 wt % before 300 °C was associated with the absorbed water or the DMC solvent, which illustrated that the sample was not dried sufficiently. It is worth noting that DMC, as the environmentally friendly solvent, is different from poisonous acetonitrile. The severe weight loss occurred from 300 to 450 °C with a weight loss more than 50% because of the degradation of carbon backbone, and the last left weight is that of the LATP particle. Under 300 °C, there is no significant loss in weight, forecasting that HSEs decomposed at temperatures over 300 °C. Because of its superior thermal stability, the HSEs could tolerate much higher operating temperatures than liquid organic electrolytes without destructing their structure. An endothermic peak was found at 54.5 °C in the curve of neat PCL, corresponding to the melting temperature (T_m). With the increasing LATP content, the melting temperature distinctively declined because of the inhibition crystallinity of the polymer (Figure 2c), which is profitable to the Li-ion movement. As we know, the migration of Li-ion happens in the noncrystalline phase,[47] the crystallinity of the PCL reduces, as exhibited by X-ray diffraction (XRD) (Figure 2d), and the increasing amorphous phase is convenient to promote elevating ionic conductivity and ion migration. Furthermore, the XRD results of the PCL and the PCL−$LiClO_4$ are shown in Figure S2. The percentage of crystallinity (χ_c) of PCL, PCL-$LiClO_4$, HSEs-20%, and HSEs-40% were 41.33, 39.63, 31.98, and 26.48%, respectively. The melting heat (ΔH_m) and the corresponding percentage of crystallinity (χ_c) of HSEs with different LATP contents are shown in Table S1. The mechanical properties of the HSEs are presented in Table S2, the mechanical strength of HSEs-40% was 5.37 MPa, and corresponding deformation was 41% while the maximum stress of HSEs-20% was 5.86 MPa, and the strain reached 117.75%.

The SEM image of HSEs with different LATP contents is shown in Figure 3. The surface morphologies of the HSEs

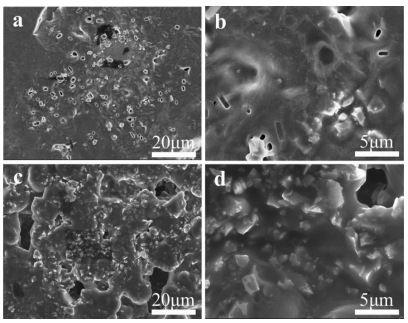

Figure 3. SEM images of (a, b) HSEs-20% and (c, d) HSEs-40%.

show that the LATP particles are embedded in the PCL matrix, and the particles in HSEs-40% are more widely dispersed in the polymer matrix compared to those of HSEs-20%, as illustrated in Figure 3. The additional EDS mappings reveal the homogenous distributions of various elements (Al, Cl, Ti, and P) in HSEs-40% (Figure S3).

The impedance of HSEs was further investigated, and the ionic conductivities of HSEs-40% and HSEs-20% are shown in Figure 4a, which shows the ionic conductivity evolution of the HSEs with the change in temperature and LATP content. The ionic conductivity of HSEs-40% was measured to be 3.64×10^{-5} S cm^{-1} at 55 °C, which is higher than that of HSEs-20% (7.78×10^{-6} S cm^{-1} at 55 °C). The ionic conductivity increased with elevating temperature, which is consistent with the law of ionic conductor. The results also indicated that the ionic conductivity of the electrolyte was higher by mixing more LATP fillers from 20 to 40 wt % content because LATP particles could suppress the crystallinity of the polymer and increase the percentage of the amorphous phase, leading to the promotion of ionic conductivity. With different LATP contents, the electrochemical window was tested by the LSV measurements, and the Li-ion transference number increased, as illustrated in Figure 4b,c. The Li-ion transference number of the HSEs-40% is 0.58, which is in contrast to the value 0.15 of HSEs-20% (Figure S4 and Table S3). The migration pathway for HSEs with different LATP amounts is shown in Figure S5. The electrochemical performance of PCL−$LiClO_4$ is shown in Figure S6 a-c, and the ionic conductivity of PCL−$LiClO_4$ was measured to be 2.36×10^{-6} S cm^{-1} at 55 °C, which is lower than that of the HSEs-40% (3.64×10^{-5} S cm^{-1} at 55 °C). In addition, the Li-ion transference number of PCL−$LiClO_4$ was 0.05, which was not satisfactory for practical applications. Also, the electrochemical stability of PCL−$LiClO_4$, HSEs-20%, and HSEs-40% by cyclic voltammetry(CV) is presented in Figure S6c−e. Moreover, the ionic conductivity of PCL−$LiClO_4$, HSEs-20%, and HSEs-40% was compared, as presented in Figure S6f.

Typically, three major factors are of importance for affecting the performance of HSEs: (1) the LATP particles decline the crystallinity of the polymer and increase the amorphous phase percentage, which is critical for facilitating the migration of Li-ions; (2) the migration efficiency of Li-ions and ionic conductivity are promoted with more migration paths and meliorates thermostability, as displayed in Figure S7a−d; (3) the PCL matrix may offer nonbonding electrons for coordination with Li-ions, which facilitates the dissociation of lithium salt. However, with the increase in the LATP content, more ceramic particles are difficult to be dispersed in the PCL matrix, and it is easy to form clusters, and it involves free-volume consumption.[6,39] In addition, more LATP particles that may induce irreversible side reactions were added in the system and caused breaking the equilibrium of charge/discharge. The symmetric battery of HSEs was tested using Li| PCL-$LiClO_4$-LATP |Li, as shown in Figure 4d. The interface of HSEs-40% with the lithium metal anode is more stable than that of HSEs-20% for over 300 h. The HSEs-40% showed a small polarization potential of 0.16 V, which was lower than that of HSEs-20% (0.91 V after 200 h), illustrating that the prominent stability and compatibility between HSEs and the lithium metal electrode were achieved for the HSEs-40%, and forecasting a relatively stable Li plating/stripping process. Most importantly, the HSEs-40% did not show any unusual condition by symmetric battery testing, which may be due to the fact that the PCL matrix and appropriate LATP particle content played an important role in the whole system for interfacial compatibility and suppressing dendrite formation or growth.[48−50]

Based on the symmetric Li battery results, the cycling tests of all-solid-state lithium batteries were further performed. The

https://dx.doi.org/10.1021/acsaem.0c02846
ACS Appl. Energy Mater. 2021, 4, 2318−2326

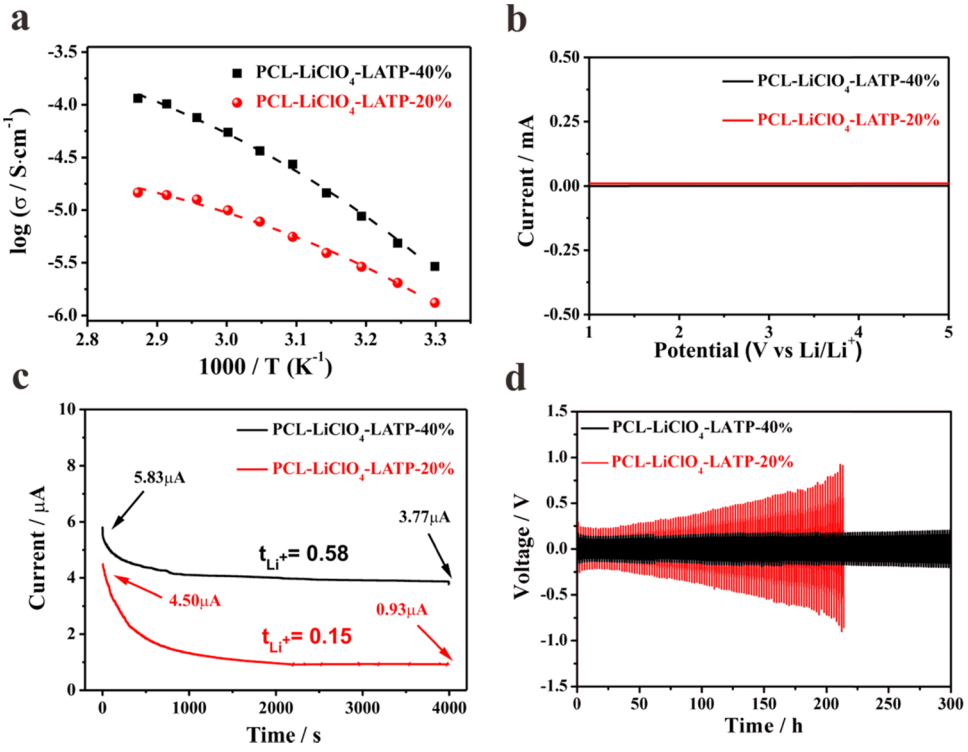

Figure 4. (a) Ionic conductivity of HSEs-40% and HSEs-20% as a function of temperature. (b) LSV curves and (c) chronoamperometry profiles of HSEs-40% and HSEs-20%. (d) Polarization voltage profiles of the symmetrical Li/HSEs/Li battery.

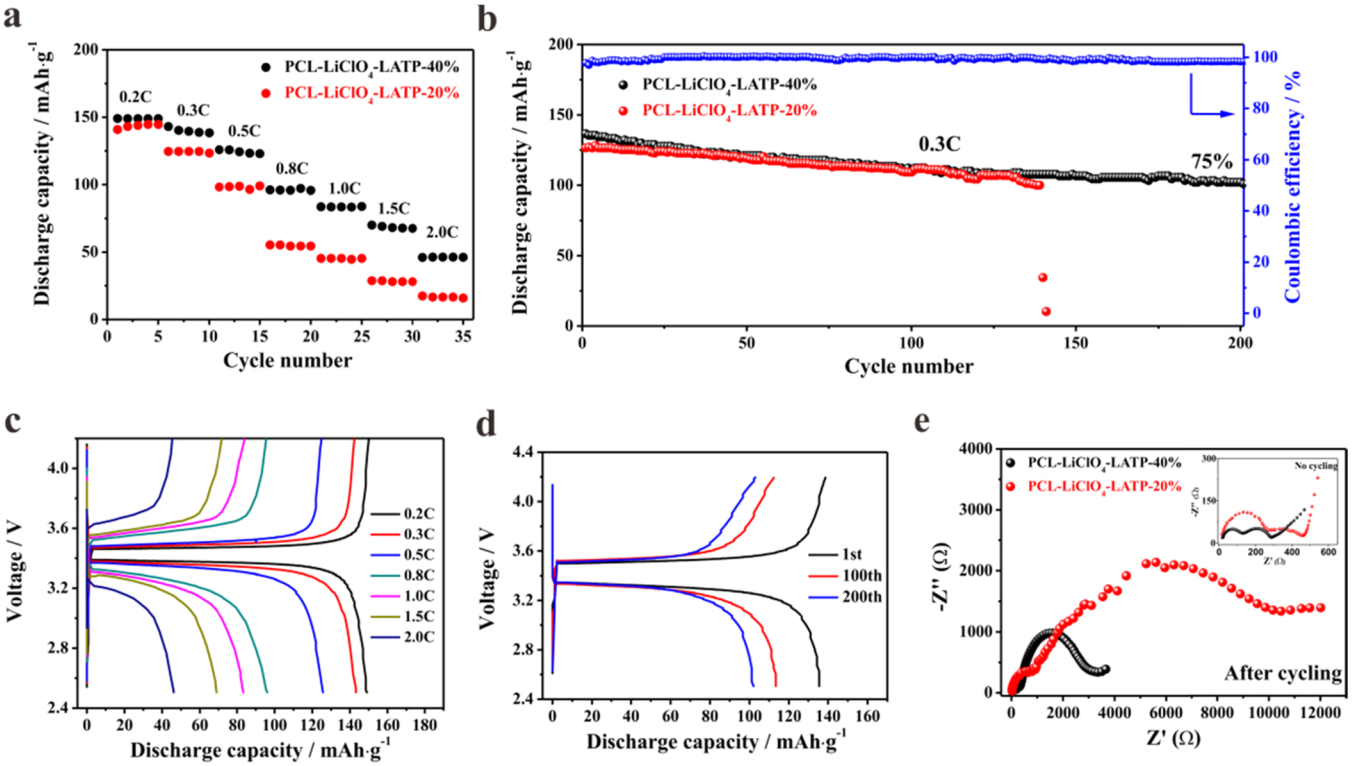

Figure 5. (a) Rate performance and (b) cycling performance of batteries with HSEs-20% and HSEs-40%. (c) Typical charge/discharge curves of batteries with HSEs-40% at various rates. (d) Typical charge/discharge curves of batteries with HSEs-40% at different cycles. (e) EIS of batteries with HSEs-20% and HSEs-40% before and after cycling.

rate performance of all-solid-state LFP| PCL-$LiClO_4$-LATP |Li batteries is displayed in Figure 5a. The all-solid-state lithium battery with HSEs-40% exhibited high discharge capacities of 149.0, 138.4, 124.3, 97.2, 83.7, 69.2, and 46.4 mAh g^{-1} at the rates of 0.2, 0.3, 0.5, 0.8, 1, 1.5, and 2 C, respectively. In comparison, the all-solid-state battery with HSEs-20%

https://dx.doi.org/10.1021/acsaem.0c02846
ACS Appl. Energy Mater. 2021, 4, 2318−2326

displayed the discharge capacities of 144.1, 124.7, 98.5, 55.3, 45.5, 28.8, and 16.7 mAh g^{-1} at the corresponding same rates. The exhibited rate performance of all-solid-state batteries with HSEs-40% is better than that of HSEs-20%, which proved the assumption that the addition of more LATP particles could promote Li-ion transmission and elevate battery performance, especially under high-rate conditions. Nevertheless, the further increase in the LATP content may induce side reactions, leading to the disequilibrium of charge/discharge processes. The charge−discharge curves of the battery with HSEs-60% (60 wt % LATP) are shown in Figure S7e where the charge capacity is higher than the discharge capacity because excess LATP particles may cause the irreversible side reaction.[13,51] In addition, the Coulombic efficiency of the battery with HSEs-60% was far below 100%, as shown in Figure S7f, and the reason may be the reduction reaction of Ti^{4+}. For HSE-60%, the side reaction was revealed by the CV curve shown in Figure S8a. The side reaction would be caused when lithium metal contacted with the LATP ceramic plate directly, as displayed in Figure S8b, as the other side of the LATP ceramic plate that did not contact with lithium metal showed no change.

The cycling performance of batteries with HSEs-40% and HSEs-20% is presented in Figure 5b. The solid-state battery with HSEs-40% showed a high initial discharge capacity of 136.6 mAh g^{-1} and good cycling performance with 75% capacity retention after 200 cycles at 55 °C. A remarkable Coulombic efficiency of nearly 100% was also observed for the battery with HSE-40%. In addition to LFP, Li-$Ni_{0.5}Mn_{0.2}Co_{0.3}O_2$ was also used as the cathode for the all-solid-state lithium battery with HSEs-40%, and the electrochemical performance is shown in Figure S9. In contrast, the all-solid-state lithium battery with HSEs-20% exhibited a lower initial discharge capacity of 126.5 mAh g^{-1}, and the discharge capacities declined sharply after 140 cycles (Figure 5b). The cycled battery cannot operate normally, which may be caused by the increase in the interfacial resistance with growing cycles at a high temperature. It is illustrated that the battery with HSEs-40% exhibits better thermal stability and higher electrochemical performance than the battery with HSEs-20% because rational LATP additives may promote the ability of thermotolerant and transfer efficiency of Li-ion, leading to elevate the electrochemical performance. The performance of the reported HSE-based all-solid-state lithium batteries is summarized in Table S4. The typical charge−discharge curves of LFP-based all-solid-state lithium batteries at various rates from 0.2 to 2 C at 55 °C are shown in Figure 5c. Figure 5d exhibits typical charge−discharge curves of the first, 100th, and 200th cycle of the LFP| PCL-$LiClO_4$-LATP |Li battery assembled with HSEs-40%. The 24.4 mAh g^{-1} capacity faded from the first cycle to the 100th cycle, while only 8.9 mAh g^{-1} capacity declined from the 100th cycle to the 200th cycle. Thus, the capacity decay rate was up to 17.9% in the first 100 cycles, which is higher than 7.9% of the subsequent 100 cycles. It is believed that the interface becomes more stable with the growing cycles to maintain long-term stability. The result forecasts that the SEI is reforming and consuming HSEs in the initial cycles. Although the capacity fades after cycles because of the loss of Li inventory and active materials, the all-solid-state lithium batteries with HSEs-40% still show favorable cycling performance and thermal stability at high temperatures. In addition, the EIS curves of HSEs-40% and HSEs-20% no-cycled samples and the sample after the cycle are shown in Figure 5e, which revealed that the capacity fading was due to the largely increased interface impedance inner all-solid-state lithium batteries with growing cycles and the resultant Li-ion transmission restriction, and the equivalent circuit of the as-prepared all-solid-state lithium batteries is shown in Figure S10. The EIS of HSEs-40% shows lower interface impedance than that of HSEs-20%, which is the crucial factor to promote the cycling performance for the all-solid-state lithium batteries with HSEs-40%. Hence, the prominent interfacial compatibility and stability of HSEs are the essential parameters for all-solid-state lithium batteries.[52−54]

In order to investigate the Li dendrite growth mechanism and the interface stability between the electrodes and HSEs-40%, the all-solid-state lithium battery with HSEs-40% was disassembled in an Ar-filled glovebox after the long cycling test. The internal structure of the battery is shown in Figure 6a,

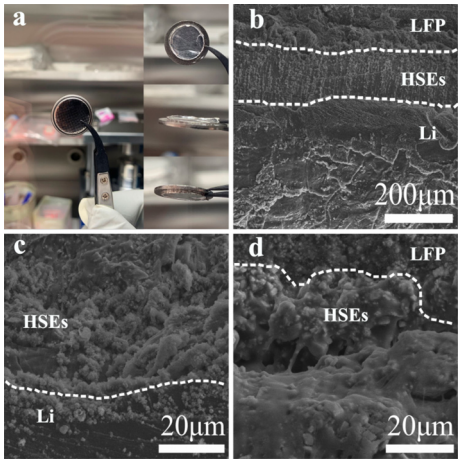

Figure 6. (a) Photographs of the all-solid-state lithium battery after disassembling. (b) SEM image of HSEs-40%-based all-solid-state lithium battery. SEM images showing (c) the interface between the electrolyte (HSEs-40%) and the lithium metal anode. (d) Interface between the HSEs-40% and the cathode.

where the HSEs-40% and the electrodes coalesce closely. The corresponding microstructure was observed evidently after heating, as exhibited in Figure 6b. During the cycling process, the interfacial adhesion between the cathode layer and the HSEs-40% membrane was reinforced accordingly, and the interfacial impedance also reduced.[55,56] The interface between HSEs-40% and the lithium metal anode is displayed in Figure 6c; the interface was flat without obvious Li dendrite formation. Furthermore, the cathode and HSEs-40% displayed favorable stability and compatibility after long cycles, as presented in Figure 6d. The structure not only reduces the interface impedance between the electrolytes and electrodes but also suppresses the growth of Li dendrites by the polymer matrix and thus protects the lithium metal anode without side reactions. The excellent interface contact and good wetting ability can promote Li-ion migration significantly and reduce the impedance of charge transfer.[57−59] Moreover, the pouch battery with HSEs-40% was fabricated to explore the practical applications.

The pouch battery that lighted the light-emitting diode (LED) at room temperature is shown in Figure 7a, demonstrating that the HSEs-40% has enough capacity to maintain working miniwatt devices. The pouch battery with HSEs-40% was well-operated when the pouch battery was

https://dx.doi.org/10.1021/acsaem.0c02846
ACS Appl. Energy Mater. 2021, 4, 2318−2326

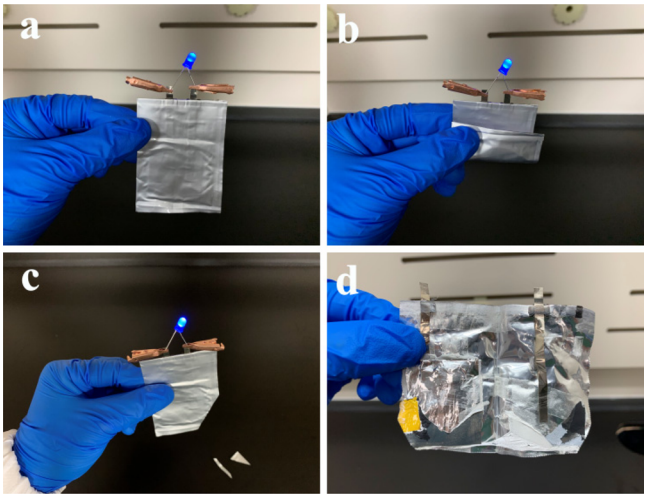

Figure 7. (a–c) Photographs of the soft-packed all-solid-state lithium battery with HSEs-40%. (d) Photograph of soft-packed all-solid-state lithium battery after disassembling without any liquid electrolyte.

under folding or even cropping, as presented in Figure 7b,c. The battery with HSEs-40% showed outstanding safety performance and application prospect compared to the liquid organic electrolyte in extreme environments, indicating that HSEs-40% hold great promise for flexible electronics. Notably, the pouch battery with HSEs-40% has no liquid solvent even after disassembling, as shown in Figure 7d, which makes a smaller battery than the liquid organic electrolyte-based battery with an equivalent capacity, and that is beneficial to elevate the energy density.

4. CONCLUSIONS

A flexible HSE was synthesized using a simple strategy, and it demonstrated a large electrochemical window (>5 V vs Li/Li^+) and excellent thermal stability. With adding 40 wt % LATP, PCL–$LiClO_4$–LATP HSEs have shown a high Li-ion transference number of 0.58, a stable interfacial contact, and a low percentage of crystallinity (χ_c) of 26.48%. The symmetric battery with HSEs-40% maintains highly stable plating/stripping cycling for 300 h under a current density of 0.12 mA cm^{-2} at 55 °C. The LFP-based all-solid-state lithium batteries utilize the HSEs-40% that exhibits a high initial discharge specific capacity of 136.6 mAh g^{-1} with a superior capacity retention of 75% after 200 cycles at 0.3 C and an excellent rate performance from 0.2 to 2 C without any liquid electrolyte. In addition, PCL as a biodegradable polymer matrix shows excellent mechanical properties and interfacial compatibility with the lithium metal anode. The outstanding performance of the HSEs-40% not only reveals that it is a very promising electrolyte candidate but also shows that the employed method could be an effective and convenient strategy to expand the family of HSEs by employing different chelating ligands and inorganic active ceramic fillers. Moreover, the all-solid-state lithium batteries with HSEs-40% demonstrate superior safety even with the cropping operation, which is a crucial step to enter the times of flexible, implantable energy-powering devices.

■ ASSOCIATED CONTENT

Supporting Information

The Supporting Information is available free of charge at https://pubs.acs.org/doi/10.1021/acsaem.0c02846.

XRD spectrum of LATP; XRD spectra of PCL and PCL–$LiClO_4$; EDS mapping of HSEs-40%; AC impedance spectra of Li/HSEs/Li batteries; schematic illustration of the migration pathway for HSEs; electrochemical performance of PCL–$LiClO_4$; the electrochemical stability and ionic conductivities of PCL–$LiClO_4$, HSEs-20%, and HSEs-40%; first charge/discharge curves with a high temperature standing of batteries with various HSEs; charge–discharge curves and the cycling performance of battery with HSEs-60%; cyclic voltammetry of HSEs-60% and the interface between the LATP ceramic plate and lithium metal; electrochemical performance of battery with HSEs-40% and $LiNi_{0.5}Mn_{0.2}Co_{0.3}O_2$; equivalent circuit of as-prepared all-solid-state lithium batteries.

The heat enthalpy and percentage of crystallinity of various electrolytes; stress–strain performance of various electrolytes; Li-ion transference number of the HSEs-40% and HSEs-20%; electrochemical performance comparison of all-solid-state lithium batteries with various HSEs (PDF)

■ AUTHOR INFORMATION

Corresponding Authors

Xiaocong Tian – *Engineering Research Center of Nano-Geomaterials of Ministry of Education, Faculty of Materials Science and Chemistry, China University of Geosciences, Wuhan 430074, China*; Email: tianxc@cug.edu.cn

Guozhong Cao – *Department of Materials Science & Engineering, University of Washington, Seattle, Washington 98195, USA*; orcid.org/0000-0001-6539-0490; Email: gzcao@u.washington.edu

Hongyun Jin – *Engineering Research Center of Nano-Geomaterials of Ministry of Education, Faculty of Materials Science and Chemistry, China University of Geosciences, Wuhan 430074, China*; Email: jinhongyun@cug.edu.cn

Authors

Yuhang Li – *Engineering Research Center of Nano-Geomaterials of Ministry of Education, Faculty of Materials Science and Chemistry, China University of Geosciences, Wuhan 430074, China*

Min Liu – *Department of Technology Centre of Dongfeng Motor Group Co. LTD, Wuhan 430058, China*

Shanshan Duan – *Engineering Research Center of Nano-Geomaterials of Ministry of Education, Faculty of Materials Science and Chemistry, China University of Geosciences, Wuhan 430074, China*

Zixian Liu – *Engineering Research Center of Nano-Geomaterials of Ministry of Education, Faculty of Materials Science and Chemistry, China University of Geosciences, Wuhan 430074, China*

Shuen Hou – *Engineering Research Center of Nano-Geomaterials of Ministry of Education, Faculty of Materials Science and Chemistry, China University of Geosciences, Wuhan 430074, China*

Complete contact information is available at: https://pubs.acs.org/10.1021/acsaem.0c02846

https://dx.doi.org/10.1021/acsaem.0c02846
ACS Appl. Energy Mater. 2021, 4, 2318–2326

Notes

The authors declare no competing financial interest.

■ ACKNOWLEDGMENTS

This work was supported by the National Natural Science Foundation of China (21975230, 51802292), Major Scientific and Technological Innovation in Hubei (2017AAA112 and 2018AAA015, 2019AAA004), Joint Fund of Ministry of Education (6141A02033239), DONGFENG Project (91224Y180014), Zhejiang Provincial Natural Science Foundation of China (LY20B010001), the Fundamental Research Funds for the Central Universities (CUG170690), and the Research Funds for Engineering Research Center of Nano-Geo Materials of Ministry of Education (NGM2019KF015).

■ REFERENCES

(1) Cheng, X. B.; Zhang, R.; Zhao, C. Z.; Zhang, Q. Toward Safe Lithium Metal Anode in Rechargeable Batteries: A Review. *Chem. Rev.* **2017**, *117*, 10403−10473.

(2) Armand, M.; Tarascon, J. M. Building Better Batteries. *Nature* **2008**, *451*, 652−657.

(3) Tarascon, J. M.; Armand, M. Issues and Challenges Facing Rechargeable Lithium Batteries. *Nature* **2001**, *414*, 359−367.

(4) Zhang, Y. H.; Lu, W.; Cong, L. N.; Liu, J.; Sun, L. Q.; Mauger, A.; Julien, C. M.; Xie, H. M.; Liu, J. Cross-linking network based on Poly(ethylene oxide): Solid Polymer Electrolyte for Room Temperature Lithium Battery. *J. Power Sources* **2019**, *420*, 63−72.

(5) Chu, S.; Majumdar, A. Opportunities and Challenges for a Sustainable Energy Future. *Nature* **2012**, *488*, 294−303.

(6) Zhang, J. J.; Zang, X.; Wen, H. J.; Dong, T. T.; Chai, J. C.; Li, Y.; Chen, B. B.; Zhao, J. W.; Dong, S. M.; Ma, J.; Yue, L. P.; Liu, Z. H.; Guo, X. X.; Cui, G. L.; Chen, L. Q. High-Voltage and Free-Standing Poly(propylene carbonate)/$Li_{6.75}La_3Zr_{1.75}Ta_{0.25}O_{12}$ Composite Solid Electrolyte for Wide Temperature Range and Flexible Solid Lithium Ion Battery. *J. Mater. Chem. A* **2017**, *5*, 4940−4948.

(7) Zhang, J. X.; Zhao, N.; Zhang, M.; Li, Y. Q.; Chu, P. K.; Guo, X. X.; Di, Z. F.; Wang, X.; Li, H. Flexible and Ion-Conducting Membrane Electrolytes for Solid-State Lithium Batteries: Dispersion of Garnet Nanoparticles in Insulating Polyethylene Oxide. *Nano Energy* **2016**, *28*, 447−454.

(8) Kimura, K.; Yajima, M.; Tominaga, Y. A Highly-Concentrated Poly(ethylene carbonate)-Based Electrolyte for All-Solid-State Li Battery Working at Room Temperature. *Electrochem. Commun.* **2016**, *66*, 46−48.

(9) Mai, L.; Yan, M.; Zhao, Y. Track Batteries Degrading In Real Time. *Nature* **2017**, *546*, 469−470.

(10) Kato, Y.; Hori, S.; Suzuki, K.; Hirayama, M.; Yonemura, M.; Iba, H.; Kanno, R. High-Power All-Solid-State Batteries Using Sulfide Superionic Conductors. *Nat. Energy* **2016**, *1*, 1−7.

(11) Zhang, J. J.; Zhao, J. H.; Yue, L. P.; Wang, Q. F.; Chai, J. C.; Liu, Z. H.; Zhou, X. H.; Li, H.; Guo, Y. G.; Cui, G. L.; Chen, L. Q. Safety-Reinforced Poly(Propylene Carbonate)-Based All-Solid-State Polymer Electrolyte for Ambient-Temperature Solid Polymer Lithium Batteries. *Adv. Energy Mater.* **2015**, *5*, No. 1501082.

(12) Ma, Y.; Ma, J.; Chai, J. C.; Liu, Z. H.; Ding, G. L.; Xu, G. J.; Liu, H. S.; Chen, B. B.; Zhou, X. H.; Cui, G. L.; Chen, L. Q. Two Players Make a Formidable Combination: In Situ Generated Poly(acrylic anhydride-2-methyl-acrylic acid-2-oxirane-ethyl ester-methyl methacrylate) Cross-Linking Gel Polymer Electrolyte toward 5 V High-Voltage Batteries. *ACS Appl. Mater. Interfaces* **2017**, *9*, 41462−41472.

(13) Wang, L. P.; Zhang, X. D.; Wang, T. S.; Yin, Y. X.; Shi, J. L.; Wang, C. R.; Guo, Y. G. Ameliorating the Interfacial Problems of Cathode and Solid-State Electrolytes by Interface Modification of Functional Polymers. *Adv. Energy Mater.* **2018**, No. 1801528.

(14) Chen, L.; Li, Y. T.; Li, S. P.; Fan, L. Z.; Nan, C. W.; Goodenough, J. B. PEO/Garnet Composite Electrolytes for Solid-State Lithium Batteries: From "Ceramic-In-Polymer" to "Polymer-In-Ceramic". *Nano Energy* **2018**, *46*, 176−184.

(15) Jung, Y. C.; Lee, S. M.; Choi, J. H.; Jang, S. S.; Kim, D. W. All Solid-State Lithium Batteries Assembled with Hybrid Solid Electrolytes. *J. Electrochem. Soc.* **2015**, *162*, A704−A710.

(16) Liu, J.; Bao, Z. N.; Cui, Y.; Dufek, E. J.; Goodenough, J. B.; Khalifah, P.; Li, Q.; Liaw, B. Y.; Liu, P.; Manthiram, A.; Meng, Y. S.; Subramanian, V. R.; Toney, M. F.; Viswanathan, V. V.; Whittingham, M. S.; Xiao, J.; Xu, W.; Yang, J. H.; Yang, X. Q.; Zhang, J. G. Pathways for Practical High-Energy Long-Cycling Lithium Metal Batteries. *Nat. Energy* **2019**, *4*, 180−186.

(17) Zhang, W.; Nie, J.; Li, F.; Wang, Z. L.; Sun, C. A Durable and Safe Solid-State Lithium Battery with a Hybrid Electrolyte Membrane. *Nano Energy* **2018**, *45*, 413−419.

(18) Li, H. Practical Evaluation of Li-Ion Batteries. *Joule* **2019**, *3*, 911−914.

(19) Xue, Z.; He, D.; Xie, X. Poly(ethylene oxide)-Based Electrolytes for Lithium-Ion Batteries. *J. Mater. Chem. A* **2015**, *3*, 19218−19253.

(20) Long, L.; Wang, S.; Xiao, M.; Meng, Y. Polymer Electrolytes forLithium Polymer Batteries. *J. Mater. Chem. A* **2016**, *4*, 10038−10069.

(21) Zhang, B. H.; Liu, Y. L.; Pan, X. M.; Liu, J.; Doyle-Davis, K.; Sun, L. Q.; Liu, J.; Jiao, X. F.; Jie, J.; Xie, H. M.; Sun, X. L. Dendrite-Free Lithium Metal Solid Battery with a Novel Polyester Based Triblock Copolymer Solid-State Electrolyte. *Nano Energy* **2020**, *72*, No. 104690.

(22) Fonseca, C. P.; Rosa, D. S.; Gaboardi, F.; Neves, S. Development of a Biodegradable Polymer Electrolyte for Rechargeable Batteries. *J. Power Sources* **2006**, *155*, 381−384.

(23) Fonseca, C. P.; Neves, S. Electrochemical Properties of a Biodegradable Polymer Electrolyte Applied to a Rechargeable Lithium Battery. *J. Power Sources* **2006**, *159*, 712−716.

(24) Eriksson, T.; Mindemark, J.; Yue, M.; Brandell, D. Effects of Nanoparticle Addition to Poly(ε-caprolactone) Electrolytes: Crystallinity, Conductivity and Ambient Temperature Battery Cycling. *Electrochim. Acta* **2019**, *300*, 489−496.

(25) Zhang, D. C.; Zhang, L.; Yang, K.; Wang, H. Q.; Yu, C.; Xu, D.; Xu, B.; Wang, L. M. Superior Blends Solid Polymer Electrolyte with Integrated Hierarchical Architectures for All-Solid-State Lithium-Ion Batteries. *ACS Appl. Mater. Interfaces* **2017**, *9*, 36886−36896.

(26) Mindemark, J.; Sun, B.; Törmä, E.; Brandell, D. High-Performance Solid Polymer Electrolytes for Lithium Batteries Operational at Ambient Temperature. *J. Power Sources* **2015**, *298*, 166−170.

(27) Wang, S.; Wang, A. L.; Liu, X.; Xu, H.; Chen, J.; Zhang, L. Y. Ordered Mesogenic Units-Containing Hyperbranched Sar Liquid Crystal All-Solid-State Polymer Electrolyte for High-Safety Lithium-Ion Batteries. *Electrochim. Acta* **2018**, *259*, 213−224.

(28) Bergfelt, A.; Lacey, M. J.; Hedman, J.; Sångeland, C.; Brandell, D.; Bowden, T. ε-Caprolactone-Based Solid Polymer Electrolytes for Lithium-Ion Batteries: Synthesis, Electrochemical Characterization and Mechanical Stabilization by Block Copolymerization. *RSC Adv.* **2018**, *8*, 16716−16725.

(29) Zhang, L.; Wang, S.; Li, J. Y.; Liu, X.; Chen, P. P.; Zhao, T.; Zhang, L. Y. Nitrogen-Containing All-Solid-State Hyperbranched Polymer Electrolyte for Superior Performance Lithium Batteries. *J. Mater. Chem. A* **2019**, *7*, 6801−6808.

(30) Imholt, L.; Dörr, T. S.; Zhang, P.; Ibing, L.; Cekic-Laskovic, I.; Winter, M.; Brunklaus, G. Grafted Polyrotaxanes as Highly Conductive Electrolytes for Lithium Metal Batteries. *J. Power Sources* **2019**, *409*, 148−158.

(31) Zuo, C.; Chen, G.; Zhang, Y.; Gan, H. H.; Li, S. Q.; Yu, L. P.; Zhou, X. P.; Xie, X. L.; Xue, Z. G. Poly(ε-caprolactone)-Block-Poly(ethylene glycol)-Block-Poly(ε-caprolactone)-Based Hybrid Polymer Electrolyte for Lithium Metal Batteries. *J. Membr. Sci.* **2020**, *607*, No. 118132.

(32) Zhao, Y. R.; Wu, C.; Peng, G.; Chen, X. T.; Yao, X. Y.; Bai, Y.; Wu, F.; Chen, S. J.; Xu, X. X. A New Solid Polymer Electrolyte

https://dx.doi.org/10.1021/acsaem.0c02846
ACS Appl. Energy Mater. 2021, 4, 2318−2326

Incorporating $Li_{10}GeP_2S_{12}$ into a Polyethylene Oxide Matrix for All-Solid-State Lithium Batteries. *J. Power Sources* **2016**, *301*, 47−53.
(33) Srivastava, S.; Schaefer, J. L.; Yang, Z.; Tu, Z.; Archer, L. A. 25th Anniversary Article: Polymer-Particle Composites: Phase Stability and Applications in Electrochemical Energy Storage. *Adv. Mater.* **2014**, *26*, 201−234.
(34) Duan, S. S.; Jin, H. Y.; Yu, J. X.; Esfahani, E. N.; Yang, B.; Liu, J.; Ren, Y. Z.; Chen, Y.; Lu, L. H.; Tian, X. C.; Hou, S. E.; Li, J. Y. Non-Equilibrium Microstructure of $Li_{1.4}Al_{0.4}Ti_{1.6}(PO_4)_3$ Superionic Conductor by Spark Plasma Sintering for Enhanced Ionic Conductivity. *Nano Energy* **2018**, *51*, 19−25.
(35) Jenkins, M. J.; Harrison, K. L. The effect of Molecular Weight on the Crystallization Kinetics of Polycaprolactone. *Polym. Adv. Technol.* **2006**, *17*, 474−478.
(36) Zhu, L.; Zhu, P.; Fang, Q.; Jing, M.; Shen, X.; Yang, L. A Novel Solid PEO/LLTO-Nanowires Polymer Composite Electrolyte for Solid-State Lithium-Ion Battery. *Electrochim. Acta* **2018**, *292*, 718−726.
(37) Liu, S.; Imanishi, N.; Zhang, T.; Hirano, A.; Takeda, Y.; Yamamoto, O.; Yang, J. Effect of Nano-Silica Filler in Polymer Electrolyte on Li Dendrite Formation in Li/Poly(ethylene oxide)-$Li(CF_3SO_2)_2N$/Li. *J. Power Sources* **2010**, *195*, 6847−6853.
(38) Yang, T.; Zheng, J.; Cheng, Q.; Hu, Y. Y.; Chan, C. K. Composite Polymer Electrolytes with $Li_7La_3Zr_2O_{12}$ Garnet-Type Nanowires as Ceramic Fillers: Mechanism of Conductivity Enhancement and Role of Doping and Morphology. *ACS Appl. Mater. Interfaces* **2017**, *9*, 21773−21780.
(39) Chen, F.; Yang, D. J.; Zha, W. P.; Zhu, B. D.; Zhang, Y. H.; Li, J. Y.; Gu, Y. P.; Shen, Q.; Zhang, L. M.; Sadoway, D. R. Solid Polymer Electrolytes Incorporating Cubic $Li_7La_3Zr_2O_{12}$ for All-Solid-State Lithium Rechargeable Batteries. *Electrochim. Acta* **2017**, *258*, 1106−1114.
(40) Diederichsen, K. M.; McShane, E. J.; McCloskey, B. D. Promising Routes to a High Li^+ Transference Number Electrolyte for Lithium Ion Batteries. *ACS Energy Lett.* **2017**, *2*, 2563−2575.
(41) Bruce, P. G.; Hardgrave, M. T.; Vincent, C. A. Steady state current flow in solid binary electrolyte cells Part 2. The effect of ion association. *J. Electroanal. Chem.* **1989**, *271*, 27−34.
(42) Zhao, C. Z.; Zhang, X. Q.; Cheng, X. B.; Zhang, R.; Xu, R.; Chen, P. Y.; Peng, H. J.; Huang, J. Q.; Zhang, Q. An Anion-Immobilized Composite Electrolyte for Dendrite-Free Lithium Metal Anodes. *Proc. Natl. Acad. Sci. U. S. A.* **2017**, *114*, 11069−11074.
(43) Lu, D. P.; Tao, J. H.; Yan, P. F.; Henderson, W. A.; Li, Q. Y.; Shao, Y. Y.; Helm, M. L.; Borodin, O.; Graff, G. L.; Polzin, B.; Wang, C.; Engelhard, M.; Zhang, J.; De Yoreo, J. J.; Liu, J.; Xiao, J. Formation of Reversible Solid Electrolyte Interface on Graphite Surface from Concentrated Electrolytes. *Nano Lett.* **2017**, *17*, 1602−1609.
(44) Cheng, X. B.; Yan, C.; Peng, H. J.; Huang, J. Q.; Yang, S. T.; Zhang, Q. Sulfurized Solid Electrolyte Interphases with a Rapid Li^+ Diffusion on Dendrite-Free Li Metal Anodes. *Energy Storage Mater.* **2018**, *10*, 199−205.
(45) Xu, L.; Tang, S.; Cheng, Y.; Wang, K. Y.; Liang, J. Y.; Liu, C.; Cao, Y. C.; Wei, F.; Mai, L. Q. Interfaces in Solid-State Lithium Batteries. *Joule* **2018**, *2*, 1991−2015.
(46) Li, D.; Chen, L.; Wang, T.; Fan, L.-Z. 3D Fiber-Network-Reinforced Bicontinuous Composite Solid Electrolyte for Dendrite-free Lithium Metal Batteries. *ACS Appl. Mater. Interfaces* **2018**, *10*, 7069−7078.
(47) Zhou, D.; Shanmukaraj, D.; Tkacheva, A.; Armand, M.; Wang, G. X. Polymer Electrolytes for Lithium-Based Batteries: Advances and Prospects. *Chem* **2019**, *5*, 2326−2352.
(48) Zhang, X.; Liu, T.; Zhang, S. F.; Huang, X.; Xu, B. Q.; Lin, Y. H.; Xu, B.; Li, L. L.; Nan, C. W.; Shen, Y. Synergistic Coupling between $Li_{6.75}La_3Zr_{1.75}Ta_{0.25}O_{12}$ and Poly(vinylidene fluoride) Induces High Ionic Conductivity, Mechanical Strength, and Thermal Stability of Solid Composite Electrolytes. *J. Am. Chem. Soc.* **2017**, *139*, 13779−13785.
(49) Chen, L.; Li, W.; Fan, L.-Z.; Nan, C.-W.; Zhang, Q. Intercalated Electrolyte with High Transference Number for Dendrite-Free Solid-State Lithium Batteries. *Adv. Funct. Mater.* **2019**, *29*, No. 1901047.
(50) Duan, J.; Wu, W. Y.; Nolan, A. M.; Wang, T. R.; Wen, J. Y.; Hu, C. C.; Mo, Y. F.; Luo, W.; Huang, Y. H. Lithium-Graphite Paste: An Interface Compatible Anode for Solid-State Batteries. *Adv. Mater.* **2019**, *31*, No. 1807243.
(51) Yang, L. Y.; Wang, Z. J.; Feng, Y. C.; Tan, R.; Zuo, Y. X.; Gao, R. T.; Zhao, Y.; Han, L.; Wang, Z. Q.; Pan, F. Flexible Composite Solid Electrolyte Facilitating Highly Stable "Soft Contacting" Li-Electrolyte Interface for Solid State Lithium-Ion Batteries. *Adv. Energy Mater.* **2017**, *7*, No. 1701437.
(52) Liang, J. Y.; Zeng, X. X.; Zhang, X. D.; Zuo, T. T.; Yan, M.; Yin, Y. X.; Shi, J. L.; Wu, X. W.; Guo, Y. G.; Wan, L. J. Engineering Janus Interfaces of Ceramic Electrolyte via Distinct Functional Polymers for Stable High-Voltage Li-Metal Batteries. *J. Am. Chem. Soc.* **2019**, *141*, 9165−9169.
(53) Zhai, H.; Xu, P.; Ning, M.; Cheng, Q.; Mandal, J.; Yang, Y. A Flexible Solid Composite Electrolyte with Vertically Aligned and Connected Ion-Conducting Nanoparticles for Lithium Batteries. *Nano Lett.* **2017**, *17*, 3182−3187.
(54) Huang, Y.; Chen, B.; Duan, J.; Yang, F.; Wang, T. R.; Wang, Z. F.; Yang, W. J.; Hu, C. C.; Luo, W.; Huang, Y. H. g-C_3N_4: An Interface Enabler for Solid-State Lithium Metal Batteries. *Angew. Chem., Int. Ed.* **2020**, *59*, 3699−3704.
(55) Chen, X. Z.; He, W. J.; Ding, L. X.; Wang, S. Q.; Wang, H. H. Enhancing Interfacial Contact in All Solid State Batteries with a Cathode-Supported Solid Electrolyte Membrane Framework. *Energy Environ. Sci.* **2019**, *12*, 938−944.
(56) Sun, F.; Dong, K.; Osenberg, M.; Hilger, A.; Risse, S.; Lu, Y.; Kamm, P. H.; Klaus, M.; Markötter, H.; García-Moreno, F.; Arlt, T.; Manke, I. Visualizing the Morphological and Compositional Evolution of the Interface of InLi-Anode|Thio-LISION Electrolyte in An All-Solid-State Li-S Cell by in Operando Synchrotron X-ray Tomography and Energy Dispersive Diffraction. *J. Mater. Chem. A* **2018**, *6*, 22489−22496.
(57) Liu, W.; Lee, S. W.; Lin, D.; Shi, F.; Wang, S.; Sendek, A. D.; Cui, Y. Enhancing Ionic Conductivity in Composite Polymer Electrolytes with Well-Aligned Ceramic Nanowires. *Nat. Energy* **2017**, *2*, 1−7.
(58) Guo, Q.; Han, Y.; Wang, H.; Xiong, S.; Li, Y.; Liu, S.; Xie, K. New Class of LAGP-Based Solid Polymer Composite Electrolyte for Efficient and Safe Solid-State Lithium Batteries. *ACS Appl. Mater. Interfaces* **2017**, *9*, 41837−41844.
(59) Fu, C. K.; Lou, S. F.; Cao, Y.; Ma, Y. L.; Du, C. Y.; Zuo, P. J.; Cheng, X. Q.; Tang, W. P.; Wu, Y. M.; Gao, Y. Z.; Huo, H.; Yin, G. P. Excellent Room-Temperature Performance of Lithium Metal Polymer Battery with Enhanced Interfacial Compatibility. *Electrochim. Acta* **2018**, *283*, 1261−1268.

https://dx.doi.org/10.1021/acsaem.0c02846
ACS Appl. Energy Mater. 2021, 4, 2318−2326